Influence of PMMA brushes grafted from GO on rheological properties of PMMA/SAN immiscible blend in shear and elongation flow

Influence of PMMA brushes grafted from GO on rheological properties of PMMA/SAN immiscible blend in shear and elongation flow

Marketa Ilcikova[a,b,c,*], Monika Galeziewska[d], Roman Kolarik[a], Miroslav Mrlik[a], Josef Osicka[a], Tomas Sedlacek[a], Miroslav Slouf[e], Sabina Krejcikova[e], Veronika Gajdosova[e], Marcin Maslowski[d], Szymon Kozlowski[d], Joanna Pietrasik[d,*,], Jaroslav Mosnacek[b,f]**

[a]*Centre of Polymer Systems, Tomas Bata University in Zlin, tr. Tomase Bati 5678, Zlin, 76001, Czech Republic*

[b]*Polymer Institute, Slovak Academy of Sciences, Dubravska cesta 9, 845 41, Bratislava, Slovakia*

[c]*Department of Physics and Materials Engineering, Faculty of Technology, Tomas Bata University, Vavreckova, Zlin, 76001, Czech Republic*

[d]*Department of Chemistry, Lodz University of Technology, Institute of Polymer and Dye Technology, Stefanowskiego 16, 90-537, Lodz, Poland*

[e]*Institute of Macromolecular Chemistry, Czech Academy of Sciences, Heyrovskeho nam. 2, Praha, 16206, Czech Republic*

[f]*Centre for Advanced Materials Application, Slovak Academy of Sciences, Dubravska cesta 9, 845 11, Bratislava, Slovakia*

[*]*Corresponding author: Centre of Polymer Systems, Tomas Bata University in Zlin, tr. Tomase Bati 5678, Zlin, 76001, Czech Republic.*

[**]*Corresponding author: E-mail addresses: ilcikova@utb.cz (M. Ilcikova), monika.galeziewska@dokt.p.lodz.pl (M. Galeziewska), rkolarik@utb.cz (R. Kolarik), mrlik@utb.cz (M. Mrlik), osicka@utb.cz (J. Osicka), sedlacek@utb.cz (T. Sedlacek), slouf@imc.cas.cz (M. Slouf), krejcikova@imc.cas.cz (S. Krejcikova), gajdosova@imc.cas.cz (V. Gajdosova), marcin.maslowski@p.lodz.pl (M. Maslowski), szymon.kozlowski@dokt.p.lodz.pl (S. Kozlowski), joanna.pietrasik@p.lodz.pl (J. Pietrasik), jaroslav. mosnacek@savba.sk (J. Mosnacek).*

ABSTRACT

In real technological processes, both shear and elongational flow is present. The material properties may differ significantly under both types of flow. Hence, they both define the final morphology and thus properties of the materials. In this work, the morphology of immiscible blends containing polymer hybrid particles was related to extensional rheological properties for the first time. The effect of various lengths of polymer brushes grafted from graphene oxide particles (GO) surface was investigated. As a polymer matrix the immiscible blend of poly(methyl methacrylate)/styrene-co-acrylonitrile ($PMMA/SAN$) was used. Thus the poly(methyl methacrylate) ($PMMA$) brushes grafted from GO (GO-g-PMMA) with various number average molar masses (M_n) of $PMMA$ brushes with respect to chain entanglement limit of freely dispersed $PMMA$ were prepared. The extensional rheological properties were affected by Mn of PMMA brushes, while the rheological properties in shear

were unchanged. Transmission electron microscopy revealed the compatibilization effect for short densely grafted brushes with Mn of 10,300 g/mol, as smaller domains were observed. On the contrary, the higher M_n $PMMA$ brushes facilitated coalescence. With increasing length of brushes, the elongational viscosity at low elongation rates ($\sim <$ 0.1 s^{-1}) decreased, which facilitated the coalescence. The increase of viscosity at higher elongation rates ($\sim >$ 0.1 s^{-1}) was not sufficient enough to cause fiber breakup and thus elongated domains were formed.

Keywords: PMMA/SAN blends, immiscible blends, polymer brushes, SI-ATRP, graphene oxide, elongational rheology, rheotens

1. Introduction

Polymer blending is a technological approach that enables the preparation of materials with novel properties, improved processability, reduced costs, or utilized recycled materials. The majority of the polymers are immiscible, therefore, in the blends, the phase separation occurs, and various morphologies are formed [**1**]. The morphology determines the final properties of the blends therefore; its control is a crucial factor to design novel materials.

The morphology is determined by composition, interfacial tension, processing condition, time, and viscoelastic properties of the melt. In common technological processes, such as melt blending or extrusion, both shear and elongation flow occur. It was revealed, that viscoelastic properties in shear and elongational flow may differ significantly [**2**]. This difference was observed to be pronounced in the case of polymers with branched structure due to multiplied entanglements [**3**].

The effect of hybrid compatibilizers on rheological properties in the elongational flow of immiscible polymer blends has not been investigated so far. The compatibilizers are used to control the polymer blends morphology through the reduction of the interfacial tension [**4**]. The hybrid compatibilizers have been intensively studied in recent years. They are formed of particle core and polymer shell. The particles' core can bring additional properties to the blend, it can provide electrical conductivity or impart magnetic properties to the blend, depending on the particle nature. It should be noted that also neat particles were used as compatibilizers [**5,6**]. However, the surface modification brings advantages in better particle dispersion, distribution, and tailored location [**7-12**]. The modification of particles can be performed prior to the composite blending or in-situ, where polymers are grafted to particles during the melt blending [**13-15**]. The synthesis of well-defined hybrids particles using reversible deactivation radical polymerization ($RDRP$) techniques provides polymer shells designed in variety of architecture. They are the most widely used techniques of particle surface modification. The RDRP enables the preparation of the polymer brushes with precisely defined architecture including molar mass, topology, and grafting density [**16**]. Thus, to tune the interactions between the freely dispersed chains of the blend matrix, the polymer brushes were tethered to particles.

Compared to neat particles, the particle polymer hybrids were reported to show significant effect on the polymer blend performance, such as electrical conductivity [**17**], thermal stability of the blend structure [**18,19**], mechanical properties including toughness or damping properties [20,21]. The compatibilization effect manifests in morphological stability against coalescence, which usually occurs during processing. As mentioned above, the shear and elongational flow occur in these processes, however, no studies providing information on how the molar mass of polymer chains tethered on the

surface of hybrid compatibilizers affects the rheological properties of the polymer blends in uniaxial flow are available so far.

Therefore, in our study, the rheological flows of $PMMA/SAN$ blend in ratio of 80/20 were investigated in the absence and presence of graphene oxide modified by $PMMA$ brushes with various lengths of $PMMA$ chains tethered on the GO surface. The findings were correlated with morphological analysis by transmission electron microscopy. The graphene oxide was grafted using surface-initiated atom transfer radical polymerization ($SI-ATRP$) of methyl methacrylate under various monomer-to-initiator ratios to modulate the molecular weight of $PMMA$ brushes. It was revealed that polymer brush molecular parameters play a significant role in compatibilization efficiency.

2. Materials and methods

2.1. Materials

Graphite powder (synthetic, $<$20 μm) was received from Sigma Aldrich. Fuming nitric acid (HNO_3), potassium chlorate ($KClO_3$) and hydrochloric acid (HCl), triethylamine (TEA, $\geq$99%), 1,1,4,7,10,10-hexamethyltriethylenetetramine (HMTETA, 97%), copper (I) chloride (CuCl, $\geq$99.995%), copper (II) chloride ($CuCl_2$, $\geq$99.999%), ethyl a-bromoisobutyrate (EBIB, 98%), α-bromoisobutyryl bromide (BiBB, 98%) were supplied by Sigma Aldrich (USA). Methyl methacrylate (MMA, $\geq$99%), was also received from Sigma Aldrich (USA) and purified by passing through the column filled with basic aluminum oxide. Solvents: tetrahydrofurane (THF), N,N-dimethylformamide (DMF), acetone (99.5%), anisole and diethyl ether were purchased from POCH S.A. (Poland). The poly(methyl methacrylate) matrix (PMMA 205) was purchased from Chi Mei (China), poly(styrene-co-acrylonitrile) (SAN Luran 388 S, 32 wt % acrylonitrile) was kindly provided by $INEOS$ Styrolution (Germany).

2.2. Methods

2.2.1. Synthesis

The graphene oxide particles were prepared according to the modified Brodie method. The procedure was adopted from the literature [**22**]. The $ATRP$ initiator BiBB was introduced onto GO surface via esterification according to the procedure described elsewhere [**23**]. The grafting of PMMA from GO-Br surface was performed according to the general procedure as followed: The solid reagents GO-Br (100 mg), $CuCl_2$ (0.014 g, 0.105 mmol) and CuCl (0.024 g, 0.245 mmol) were added to Schlenk flask. The flask was closed, evacuated and back filled with argon three times. The liquid reagents were purged with argon and then added to Schlenk flask under argon flow: EBIB (0.067 mmol, 0.098 mL), HMTETA (0.351 mmol, 0.096 mL), MMA (0.14 mol, 15 mL) and anisole (15 mL). Then the reaction flask was immersed in an oil bath heated to 80 °C. The reaction was stopped after 6 h by opening the flask and diluting the reaction mixture with acetone. The GO-g-$PMMA$ hybrid was purified by filtration. The diluted reaction mixture was passed through 0.45 im $PTFE$ filtration membrane and washed with acetone (100 mL). Then the product was dispersed in DMF (50 mL), filtered and washed with acetone. This procedure was repeated twice. Finally, the product was washed with diethyl ether and dried in a vacuum oven at 40 °C and 10 mbar overnight.

2.2.2. Preparation of polymer blends

$PMMA$, SAN as well as filler were dried before processing, 60 °C at 20 mbar overnight. The blends were prepared by melt mixing using internal mixing device Mixer N50 (Brabender GmbH & Co. KG, Germany) at 150 ° C, and rotor speed 45 rpm. The 50 g of $PMMA/SAN$ in weight ratio of 80/20 was added to preheated chamber followed by the addition of filler. The melting stopped after approx. 9 min, when torque reached a constant value.

2.2.3. Characterization

Molecular parameters of $PMMA$ grown from free initiator: number average molar mass (M_n) and distribution of molar masses (Đ), were determined using gel permeation chromatography (GPC). GPC measurements were conducted with a Wyatt instrument equipped with one guard column and two columns from PSS, differential refractometer. DMF with the addition of 10 mg/L LiBr was used as an eluent, the flow rate equals to 1 mL/min and the measurement temperature was 45 °C. $PMMA$ standards were used for calibration.

The content of the organic fraction in GO-g-$PMMA$ hybrids was determined by thermogravimetric analysis (TGA) performed using TGA/ DSC1 equipment from Mettler Toledo LLC (USA). Hybrids were heated in the temperature range from 25 °C to 600 °C with a heating rate of 10 °C-min^{-1}, under argon atmosphere.

The morphology of the samples was visualized by transmission electron microscopy (TEM) using a microscope Tecnai G2 Spirit Twin (FEI; Czech Republic). The ultrathin sections for TEM analyses were prepared by ultramicrotomy at room temperature (ultramicrotome Ultracut UCT; Leica, Austria). The prepared sections were stained in RuO4 vapors for 2 h in order to increase contrast of the minority SAN phase. The stained samples were observed in TEM using bright field imaging at the accelerating voltage of 120 kV.

The shear viscosity of the prepared samples was characterized using a rotational rheometer Anton-Paar MCR 502 at 210 °C under normal pressure in an inert nitrogen atmosphere. Measurements have been performed with 25 mm parallel-plate measuring system oscillating at constant 1% deformation (defined from the measured linear viscoelastic regime) with angular frequency sweep decreasing from 300 s^{-1} to 0.0125 s^{-1} and vice versa to verify the thermal stability of the sample. The error of the measurement was less than 5%.

The uniaxial extensional viscosity of the prepared samples was characterized using a high-pressure capillary rheometer Goettfert Rheograph RG 50 with a Rheotens device at 210 °C. During the experiment, a polymer melt strand was extruded through a capillary with a length of 20 mm and a diameter of 2 mm at constant piston speed equal to 0.25 mm-s-1. Such extruded melt strand was then drawn by a pair of rotating wheels with a corrugated surface, which are fixed to a very sensitive balance system. The distance between the end of the capillary and the center of wheels describes a strand length (length of spinline) that was set to 100 mm for all the performed experiments. Then, the drawdown velocity was linearly increased from an initial speed of 14.1 mm-s-1 with a constant acceleration rate of 5 mm s^{-2} until the extended polymer strand breaks at a certain speed. Then, drawdown force as a function of drawdown velocity is reached and such an experiment is then repeated at least five times. With the help of this record, the melt strength (determined from the achieved maximum force of the drawn melt) and drawability (determined from the achieved maximum wheels speed before the melt strand break) can be defined. Finally, uniaxial extensional viscosity is

evaluated according to the set of equations derived from the Wagner model [**24**]. It should be noted that Wagner model considers shift factor depending on capillary L/D ratio, length of spinline, and either die exit velocity and various melt temperature or wall shear stress. However, in this work, the approach of determining the elongational viscosity is based only on the uniform processing conditions defined above.

Sample preparation for rotational rheology measurements was performed using hot pressing at 210 °C under 10 MPa pressure for 7 min (plus 7 min preheating) to obtain sheet of 1 mm thickness. The samples in the form of disks of 25 mm diameter were cut from the sheet using laser saw. In case of capillary rheology, samples were prepared in the form of solid polymer pellets or pieces by cutting of the sheets prepared by hot press. Before all rheological measurements, samples were dried at 80 °C at 15 mbar overnight.

3. Results

3.1. Synthesis of GO-g-PMMA hybrids

The GO-g-PMMA hybrids were synthesized under SI-ATRP conditions. PMMA brushes of different Mn were prepared. The molecular parameters of brushes tethered on the GO-g-PMMA hybrids can be found in **Table 1**. Based on the TGA analysis (see **Fig. S1**), the content of polymer in GO-g-PMMA was estimated. The polymer decomposition interval was observed between 230 °C and 430 °C. The content of the polymer was estimated to be 27 wt %, 27 wt % and 34 wt % for GO-PMMA10, GO-PMMA18, and GO-PMMA37 hybrids, respectively. The knowledge of the amount of grafted polymer and surface area of GO (BET analysis, 9.04 $m^2\ g^{-1}$ [**18**]) enables to calculate a grafting density according to the literature [**18**]. In all hybrids the grafting density was high enough to expect stretched polymer brushes [**16**].

The range of Mn of PMMA brushes was designed to generate either physical interface interactions of the low M_n brushes hybrids with matrix or entanglements between high M_n brushes and polymer matrix chains. Freely dispersed $PMMA$ chains are known to form entanglements above reaching M_n of 16,000 g mol^{-1} [**25**]. The molar mass of matrix blend components $PMMA$ and SAN was characterized by GPC in DMF on $PMMA$ and PS standards, respectively. $M_n$of $PMMA$ was 40,200 g/mol and Đ 3.92, M_n of SAN was 152,400 g/mol and Đ 2.00. Both polymers allow to form entanglements.

Table 1 Molar ratios of reagents, reaction conditions, and monomer conversion determined by $^1H\ NMR$; records of number average molar mass (M_n) and dispersity (Đ) determined by the GPC of free polymers and polymer content of the prepared hybrids determined by TGA. In all reactions EBiB:CuCl:$CuCl_2$:HMTETA = 0.95:0.35:0.15:0.5 was used and the reactions were performed at 80 °C. 50 vol % of anisole as solvent was used in all reactions except GO-PMMA37, where 30% was added.

Entry	Molar ratios MMA:EBiB	GO–Br (wt.%)	Time (h)	Conv. %)	M_n[a] (g mol^{-1})	$Đ$[a] (–)	Polymer content (wt. %)	Grafting Density (chains/nm^2)	Sample Label
1	200:0.95	0.7	6	56	10,300	1.10	27	1.75	GO-PMMA10
2	150:0.95	9.1	66	94	17,800	1.10	27	1.01	GO-PMMA18
3	500:0.95	2.8	48	71	36,800	1.13	34	0.62	GO-PMMA37

[a]Determined by GPC of PMMA chains grown from the sacrificial initiator (EBiB).

The situation becomes more complex when polymers are attached to surfaces. Then the limit of entanglement is shifted to higher M_n. The two conformational regimes were suggested for the polymer brushes grafted from spherical particles, the stretched chains and relaxed chains conformation for which the entanglements are possible. The transition from stretched chains to relaxed chains occurs

at a certain distance from the particle core. The distance is increasing with the diameter of the particle core, grafting density and decreases with excluded volume [**16**]. In the case of planar surfaces, more conformations are possible. Too densely grafted chains are not able to form entanglements even at high DP when grafted from planar surfaces. However, it can be assumed, that the relaxed conformations are preferably closed to the edges of the particles, and thus entanglements can be present to some extent there.

The polymer blends with identical concentration of GO-g-PMMA hybrids, 0.5 wt % were prepared. Considering the polymer content in GO-g-PMMA hybrids, 0.37 wt % (187 mg) of GO was used for preparation of $PMMA/SAN$ blend filled with unmodified GO as a reference sample.

The low concentration of the particles was selected to obtain systems, where elongation flow will be affected while the shear properties would be affected minimally. It was already described with literature by using copolymers as compatibilizers [**26**]. The effect of unmodified two-dimensional filler was investigated mostly in the concentrations up to 1 wt % [**5,8**] and even when the studies were done in the range of 1-9 wt%, it was concluded that the lowest studied concentration of 1 wt% was sufficient to observe the effects [**6**]. Recent studies with modified GO-g-PS were also done at 0.5 wt% of filler loading [**20**]. Therefore, in this study the same filler concentration was used and the attention was paid on the effect of the length of grafted polymer chains.

4. Morphology and particle location

The $PMMA/SAN$ blends can be miscible and immiscible depending on the composition and temperature. If AN units content in SAN is in the range of 9-30 wt%, the blend is miscible [**27**]. In this study, the content of AN in SAN corresponded to 32 wt% and $PMMA/SAN$ ratio was 80/20. The final blends were immiscible and all systems exhibited particulate morphology, as proved in **Fig. 1**. We note that the samples were stained with RuO_4 vapors, which colored the minority SAN phase dark.

The morphology of all $PMMA/SAN$ systems is summarized in **Fig. 1**. The neat $PMMA/SAN$ blend exhibited a fine and homogeneous structure (**Fig. 1**a-c). The addition of non-modified GO as well as the addition of $GO-PMMA18$ and $GO-PMMA37$ hybrids (with longer $PMMA$ chains grafted on GO surface) resulted in the blends with bigger domains (**Fig. 1**d-f and **Fig. 1**j-o). In contrast, the addition of $GO-PMMA10$ hybrid (with shorter $PMMA$ chains) displayed finer morphology (**Fig. 1**g-i). This effect was connected with the localization of the filler, as discussed below.

The neat, non-modified GO particles were always found in SAN phase as illustrated in **Fig. 2**a. They tended to form agglomerates of variable sizes, ranging from quite small to substantially larger, as documented in **Fig. 2**a. The location of GO-g-PMMA hybrids was affected by the brush length. The $GO-PMMA10$ hybrids (with the shortest $PMMA$ brushes) were mostly at the $PMMA/SAN$ interface as exemplified in **Fig. 2**b. Due to the shape of the two-dimensional particles, not whole their surface was at the interface, part of the particles was also localized in the $PMMA$ phase. With increasing molar mass of $PMMA$ brushes the GO-g-PMMA particles appeared both on the $PMMA/SAN$ interface and in $PMMA$ phase, as evidenced in **Fig. 2**c. The micrographs in **Fig. 2** show representative images, but it should be mentioned that the filler occasionally formed quite large agglomerates in the micrometer scale, especially in the case of non-modified GO platelets and, to a lesser extent, also in the systems with GO platelets with longer $PMMA$ brushes ($GO-PMMA18$ and $GO-PMMA37$).

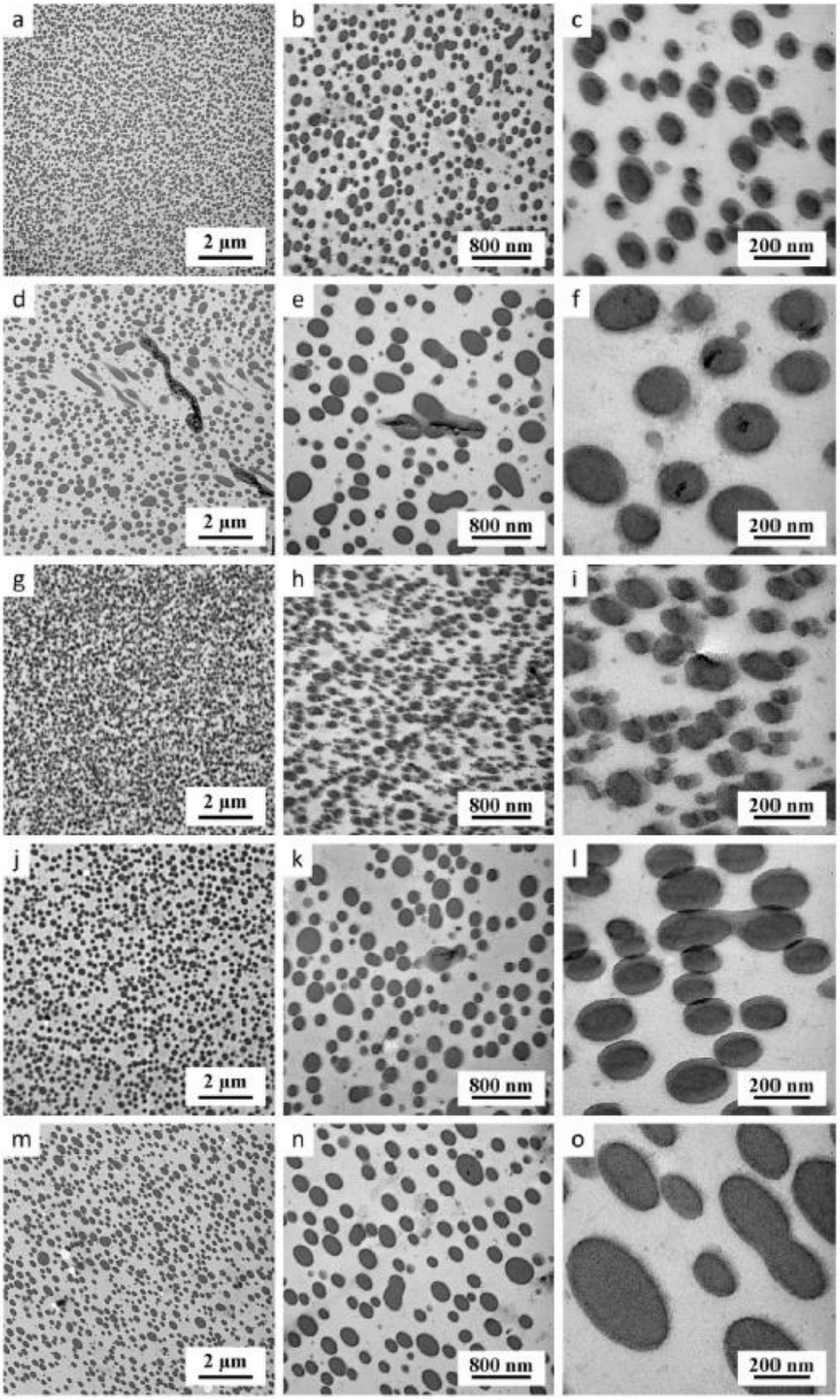

Fig. 1. TEM micrographs showing the morphology of $PMMA/SAN$ 80/20 blend and its composites: (a-c) neat $PMMA/SAN$ blend, (d-f) composite with unmodified GO, (g-i) composites with GO-g-$PMMA$ hybrids 10,300 g/mol, $GO-PMMA10$, (j-l) composites of GO-g-PMMA hybrids 17,800 g/mol, $GO-PMMA18$, (m-o) GO-g-PMMA hybrid 36,600 g/mol, $GO-PMMA37$.

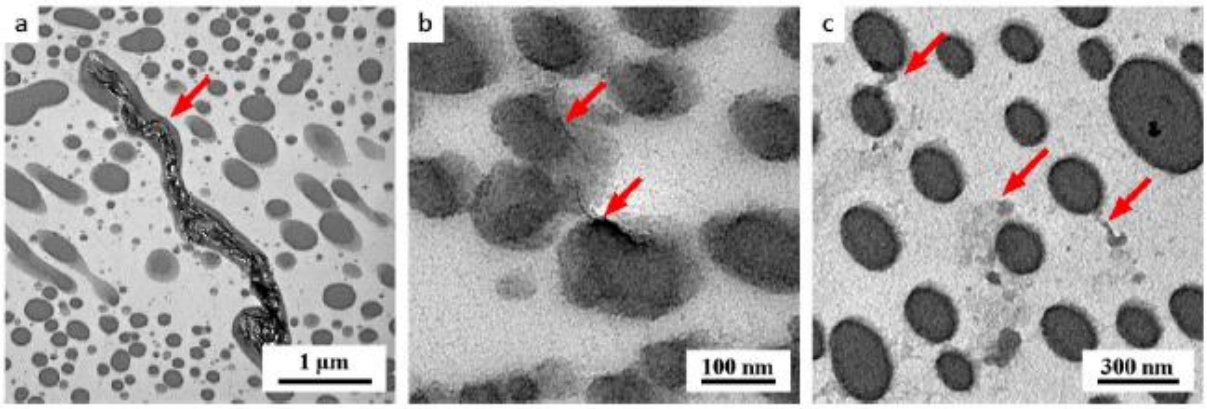

Fig. 2. TEM micrographs of $PMMA/SAN$ blends filled with (a) non-modified GO, (b) GO-g-PMMA grafted with 10,300 g/mol brushes ($GO-PMMA10$), and (c) GO-g-PMMA grafted with 36,600 g/mol brushes ($GO-PMMA37$). For non-modified GO, the filler is inside the SAN particles, for shorter brushes (b) the filler is mostly on the interface, and for the longest brushes (c) the filler is both on the interface and in the matrix. As the contrast of filler and RuO_4-stained SAN particles with respect to PMMA matrix was similar, the location of the filler is marked with red arrows. (For interpretation of the references to color in this figure legend, the reader is referred to the Web version of this article.)

The fact that $PMMA/SAN/GO-PMMA10$ systems (**Fig. 1**d-f) contained the filler on the interface was associated with their finest morphology in comparison with the blends filled with non-modified filler ($PMMA/SAN/GO$; **Fig. 1**g-i), and systems containing GO with longer brushes ($PMMA/SAN/GO-PMMA18$ and $PMMA/SAN/GO-PMMA37$; **Fig. 1**j-o).

To confirm the TEM observations, the particles' location was predicted based on wetting parameters. The details of the measurement can be found in SI. The calculations suggest that GO is situated in SAN phase, H1 (Mn = 10,300 g/mol) at the interface, the rest fillers in PMMA. The results are summarized in Table 2.

The results revealed that with increasing Mn of grafted PMMA brushes, the particles tend to locate in PMMA phase. It also correlates with the observed effect on SAN domains shape. It should be noted that the phase shape and orientation are related to the shear and elongation field, and also shear time and elongation time, and time after stopping the shear or elongation. The elliptic shape phases are commonly observed. The TEM images were performed on the polymer strand just releasing the capillary of the rheometer. The samples were exposed to the same forces, the differences are pointed. While the neat PMMA/SAN blend shows symmetric spherical domains, the composite with GO-PMMA18 and GO-PMMA37 hybrid formed rather oval SAN domains. It may be caused by the increased viscosity of the PMMA phase, due to the presence of GO-g-PMMA hybrids, as illustrated in Scheme 1. Similar effect of viscosity of the continuous phase on the morphology evolution during melt blending was observed in immiscible PE/PLA blend [26].

5. Rheology

5.1. Shear rheology

Rheology enables to study the effect of filler addition on the performance of polymer blends and also reflects the effect on polymer blend morphology [**12,19,28,29**].

The rheology in shear flow was measured and angular frequency dependence of storage modulus G'(ω) and viscosity $\eta^*(\omega)$ is plotted in **Fig. 3**a and b, respectively. The G'(ω) plot shows a shape typical for

immiscible blends dispersed morphology, i.e. shoulder in a terminal zone (low frequencies) [**30,31**]. All samples exhibit the same shape, thus the same morphology, and it correlates with TEM observations. A tiny effect of various filler types is observable in both plots. In G'(ω), the difference is visible only at low frequencies, where the neat GO particles slightly decrease the G'(ω) of PMMA/SAN blend (**Fig. 3**a). A similar trend is observable in η^* (ω) (**Fig. 3**b). The G(rn) and tf*(w) plots are not sensitive to varied polymer brush architecture, the compatibilization effect was not manifested in these plots [**31**]. Therefore, the Cole-Cole and weighted relaxation time spectra were plotted to observe the difference in rheological performance better (**Fig. 4**).

Table 2 Wetting parameter for PMMA/SAN/filler blends.

Filler	D_	Filler location
GO	−19.72	SAN
GO-PMMA10	−0.02	interface
GO-PMMA18	1.90	PMMA
GO-PMMA37	2.32	PMMA

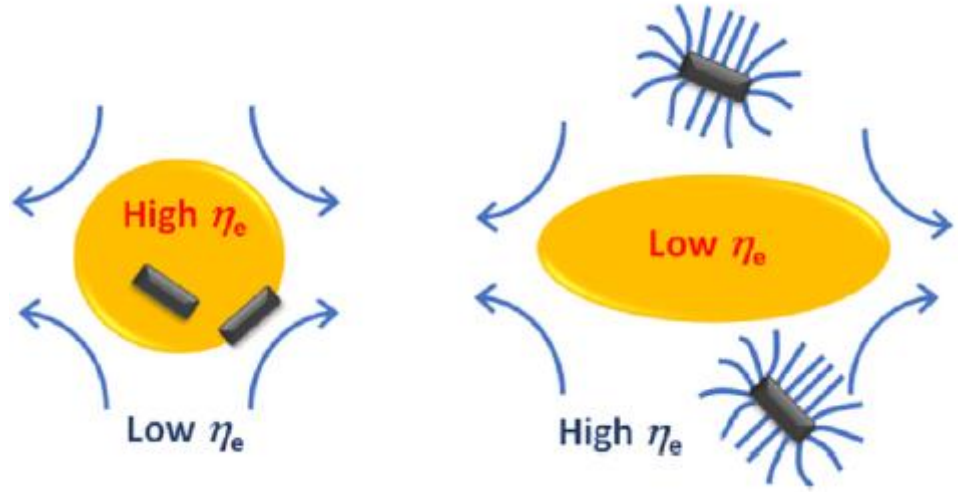

Scheme 1. Droplet stretching in elongational flow. Left) High viscosity droplet in low viscosity matrix resists the stretching due to low stress transfer. Right) Low viscosity droplet is stretched in high viscosity matrix due to high stress transfer [**26**].

Cole-Cole plot is a dependence of variables of complex viscosity η'' vs η', where $\eta^* = \eta'$-iη''. These plots enable to investigate the morphology of two-phase systems more deeply [**32**]. In the case of immiscible polymer blends, a typical semicircle shape is observed for blend components at low η', while the contribution of the interface at high n appears as a tail or another arc [**31**].

This tail is not observed in $PMMA$ or SAN homopolymers, **Fig. 4**a.

The two semicircles are observed in all blends (**Fig. 4**a). The shape of semicircles was affected by the addition of filler. The left semicircle is related to the relaxation of polymers in composites generally. The addition of $GO - PMMA37$ resulted in an increase of diameter. This effect could be caused by the polymer brushes tethered on $GO - PMMA37$ hybrids, which were long enough to provide the location of hybrids in $PMMA$ phase as was observed by TEM. Contrary to that, the neat GO resulted in a decrease of diameter, that reflects the decrease of elastic energy of the composite. TEM images showed the presence of GO in SAN phase. When focused on the relaxation of dispersed domains, the

SAN domains exhibit a significant decrease of elasticity compared to the neat matrix. The neat GO thus acted as a softener in SAN domains.

For better comparison, the effect of grafting can be quantified by calculation of relaxation time. The relaxation times are well observable in the relaxation time dependence of weighted relaxation time spectra (**Fig. 4**b). These plots enable to separate the contributions of the relaxation of interphase and components [**33-35**], since it magnifies the slow processes and thus the interfacial relaxation is more visible. The calculation was performed according to Equation (**1**) [**36**].

$$H(\tau) = G' \left[\frac{d \log G'}{d \log \omega} - \frac{1}{2}\left(\frac{d \log G''}{d \log \omega} \right)^2 - \frac{1}{4,606} \frac{\partial^2 \log G''}{\partial (\log \omega)^2} \right]_{\tau = \frac{\sqrt{2}}{\omega}} \qquad (1)$$

The relaxation of blend components is visible at short relaxation times, with peak maxima of τ close to 1s.

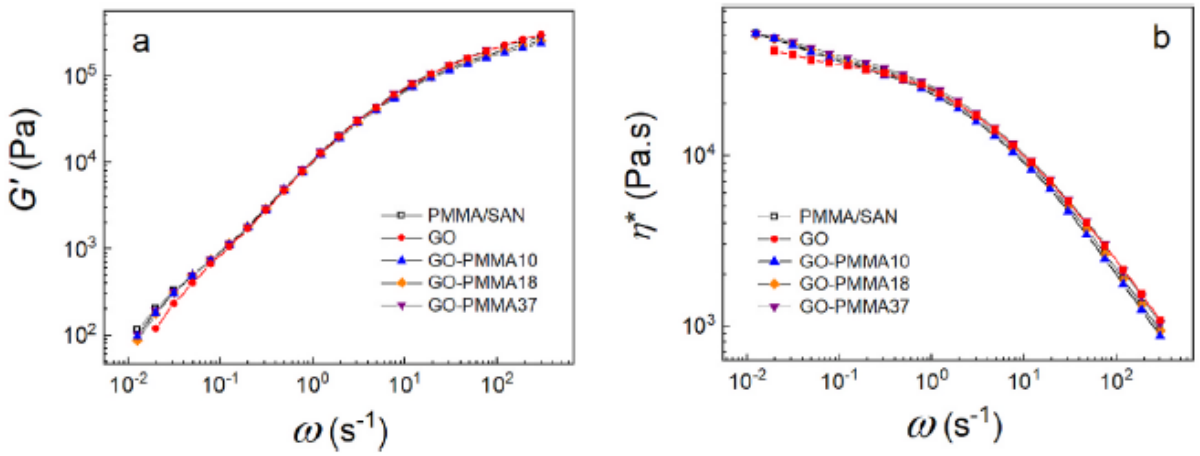

Fig. 3. Angular frequency dependence of (a) storage modulus G'(ω) and (b) complex shear viscosity $\eta^*(\omega)$ of $PMMA/SAN$ blend and its composites. The $PMMA/SAN$ composites filled with GO-g-PMMA grafted with M_n 10,300 g/mol, 17,600 g/mol brushes and 36,600 g/mol brushes are labelled as $GO-PMMA10$, $GO-PMMA18$ and $GO-PMMA37$, respectively.

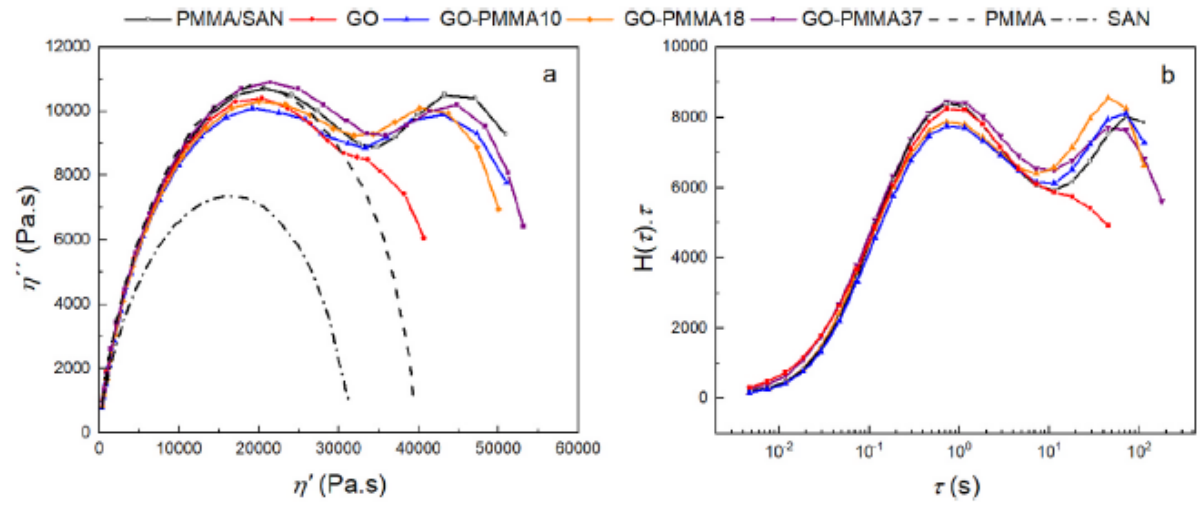

Fig. 4. Cole- Cole plot (a) and weighted relaxation time spectra (b) of $PMMA/SAN$ blend and its composites filled with neat GO, GO-g-PMMA grafted with 10,300 g/ mol brushes ($GO-PMMA10$), GO-g-PMMA grafted with 17,600 g/mol brushes

($GO-PMMA18$), and GO-g-PMMA grafted with 36,600 g/mol brushes ($GO-PMMA37$). Cole-Cole includes also spectra of neat $PMMA$ and SAN homopolymers.

The peak at higher relaxation times with peak maxima at 50s is associated with relaxations of domains. Compared to the neat $PMMA/SAN$ blend the presence of GO shifts the maximum of relaxation time significantly towards a shorter relaxation time, showing a maximum at 17s. The presence of GO particles in SAN phase resulted in faster relaxation, thus GO acts as a plasticizer of SAN phase. All types of hybrids also shift the relaxation of domains also to shorter relaxation times compared to neat $PMMA/SAN$ blend (**Table 3**). The difference between $GO-PMMA10$ and both $GO-PMMA18$ and $GO-PMMA37$ could be associated with particles' location. While $GO-PMMA10$ is predicted to locate at the interface, the relaxation here is suppressed due to the presence of particles. The $GO-PMMA18$ and $GO-PMMA37$ hybrids were observed more in $PMMA$ phase and less at the interphase, thus the plasticizing effect is slightly more pronounced. In addition, the longer $PMMA$ chains, grafted on the surface in the $GO-PMMA37$, can lead to a higher probability of entanglement with $PMMA$ matrix and thus decrease the plasticizing effect compared to $GO-PMMA18$.

The results show that the shear rheology enables to observe the effect of polymer grafting compared to neat matrix and unmodified filler. The effects of polymer brushes with different molecular structures manifest predominantly at low shear rates, at the limits of shear rheology. To investigate the effects of polymer brushes length at low deformation rates the elongational rheology was performed.

Table 3 Relaxation time of $PMMA/SAN$ blend and hybrid composites.

Sample	PMMA/SAN	GO-PMMA10	GO-PMMA18	GO-PMMA37
τ_{max} (s)	72.5	71.2	48.0	55.5

5.2. Elongational rheology in uniaxial extension

The elongational rheological properties in uniaxial extension were measured by using Rheotens experiment. The design of the experiment is depicted in **Scheme 2**. Here, the drawdown force (F) needed for elongation of an extruded filament was measured as a function of the draw ratio (V). The detailed description of the experiment can be found in SI.

Experimental data in the form of drawdown force dependence on the velocity of rotating wheels were used for the evaluation of uniaxial extensional viscosity. The data were fitted according to the several equations presented in Wagner model [**37**] combined with the power-law model. The detailed description of data processing is shown in SI.

As a result, the apparent elongational viscosity dependence on the elongational rate could be plotted (**Fig. 5**). The Newtonian plateau values are followed by shear thickening and a decrease in viscosity with an increasing elongational rate. The shear thickening appears when more interactions or entanglements are formed than destroyed. At the yield point, the polymer chains are mostly disentangled and viscosity decreases. The significant effect of polymer grafting can be seen. At low elongational rates (below $\sim$ 0.1 s^{-1}) the viscosity drops with filler addition. With increasing M_n of

brushes the Newtonian plateau provides lower values, and the plateau is broadened to higher elongational rates.

The ratio of maximal uniaxial extensional viscosity in yield and zero uniaxial extensional viscosity can be expressed as a strain hardening [**38**], and the values are summarized in **Table 3**. This parameter contributes to an explanation for morphological evolution during processing. During uniaxial extension, the morphology of the immiscible blend is affected by coalescence and fiber breakup. In the case of coalescence, the domains approach each other and then they collide to form a bigger domain. To perform this, the domains must squeeze out the matrix fluid, make a thin film, that has to rupture, and then the domains may join (**Scheme 3**).

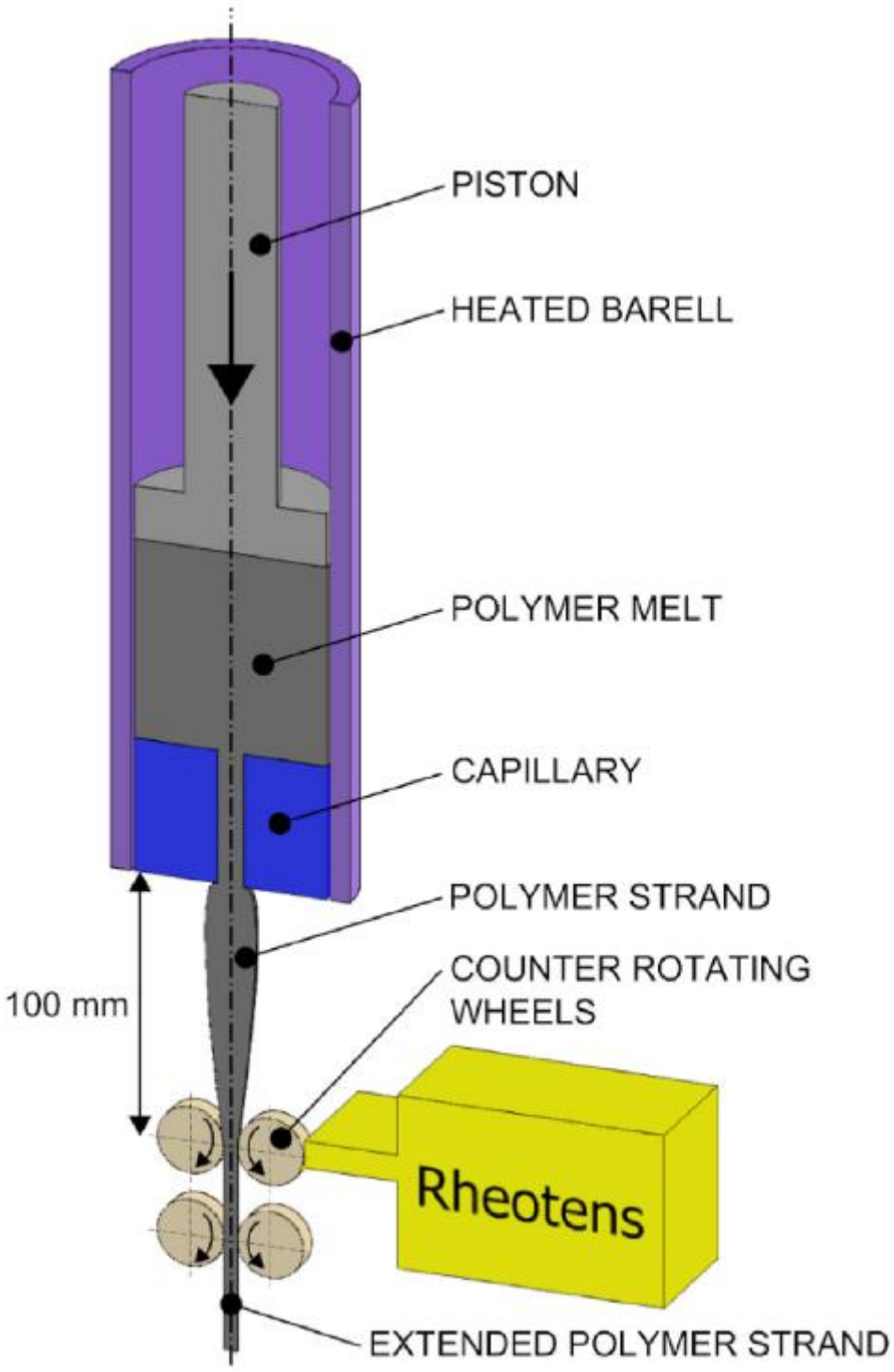

Scheme 2. Experimental setup description of the Rheotens test.

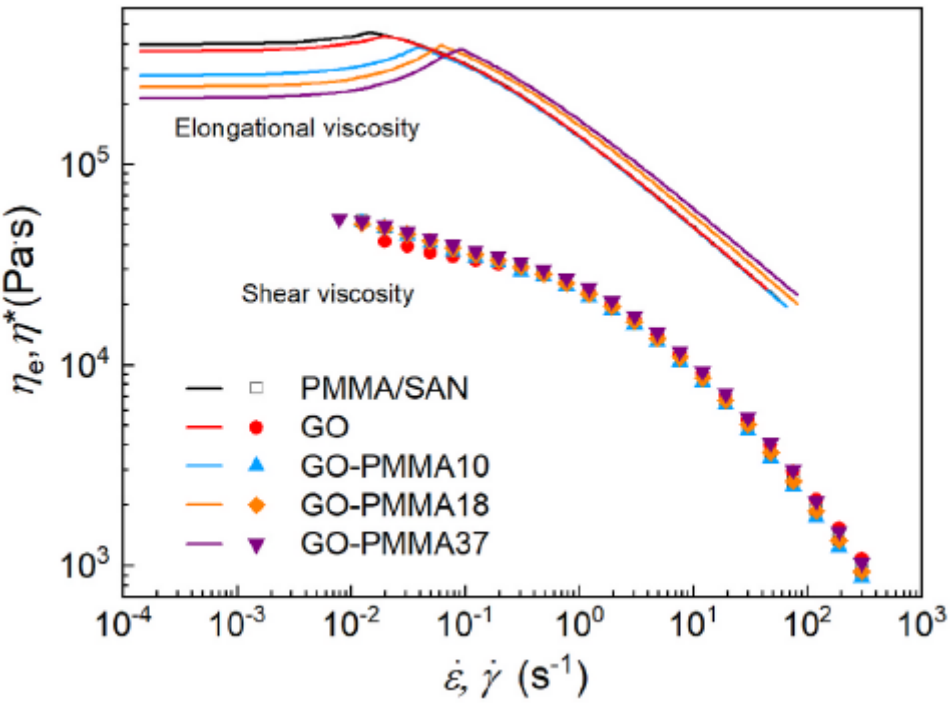

Fig. 5. Apparent elongational viscosity in dependence of elongational rate of $PMMA/SAN$ blend 80/20 and its composites filled with unmodified GO or GO-g-PMMA hybrids with various M_n of $PMMA$ brushes, in comparison to shear viscosity in dependence of shear rate, all measured at 210 °C. The $PMMA/SAN$ composites filled with GO-g-PMMA grafted with M_n 10,300 g/mol, 17,600 g/ mol brushes and 36,600 g/mol brushes are labelled as $GO-PMMA10$, $GO-PMMA18$ and $GO-PMMA37$, respectively.

This happened with the addition of $GO-PMMA18$ and $GO-PMMA37$, where bigger elongated domains were observed by TEM. On the other hand, the addition of $GO-PMMA10$ resulted in rather smaller domains, thus rather fiber breakup was detected. Literature suggests that a strainhardening matrix fluid resists the draining flow presented in step b, thereby reducing the coalescence [**26**]. However, in the case of the composites discussed herein, the strain-hardening effect was balanced with a significant drop of elongational viscosity at low elongation rates. The low viscosity at elongation rates below ~10^{-1} facilitated coalescence, with increasing rate the strain-hardening effect manifested, i.e. enhancement of viscosity, however in the case of $GO-PMMA18$ and $GO-PMMA37$ only resulted in elongation of domains. While in the case of $GO-PMMA10$ the fiber breakup was possible. It was expected due to the location of particles at the interface, where they stabilized the morphology and prevented the domains' coalescence.

The results showed that GO and especially GO-g-PMMA acted as softeners. It was proved by measuring T_g that shifts to lower temperatures with increasing length of brushes (**Fig. S3**). This is in good agreement with previously described observation for short densely grafted brushes [**18,39**]. The clear evidence is provided by investigation of rheological properties in uniaxial extension rather than in shear flow.

The direct comparison of both methods is shown in **Table 4**. Here the values of Newtonian shear viscosities η_0, Newtonian viscosity in uniaxial extension (η_{e0}), maximal uniaxial extensional viscosity (η_{emax}), strain hardening parameter (SH) of $PMMA/SAN$ blend and composites are listed. The values for elongation viscosity in Newtonian region (η_{e0}) could be obtained from **Fig. 5**, based on Wagner and the power-low model. The values of Newtonian viscosities in shear flow were fitted by Carreau-Yasuda model [**40**]. The Carreau-Yasuda model for simple shear flow can be used in the following form:

$$\eta = \eta_0 \bullet [1 + (\lambda \bullet \dot{\gamma})^a]^{\frac{n-1}{a}} \quad (6)$$

where η_0, λ, γ and n are zero shear viscosity, relaxation time, shear rate, and power law exponent, respectively. A dimensionless parameter α characterizes the sharpness of the transition between the zero shear viscosity region and the power law region.

It is also obvious that the ne0 for $PMMA/SAN$ blend decreased after the addition of GO and more significantly after the addition of GO-g-PMMA. In addition, the values of ne0 decreased with increasing M_n of $PMMA$ brushes achieving the most significant decrease for $GO - PMMA37$ sample, equal to 46%. On the other hand, η_0 of $PMMA/SAN$ increased after the addition of $GO - PMMA37$ by 2%.

The results manifest the importance of investigations of the complex rheological performance of polymer blends filled with hybrid particles. The effect of the brush architecture was only detectable in uniaxial extension, where significant effects were identified.

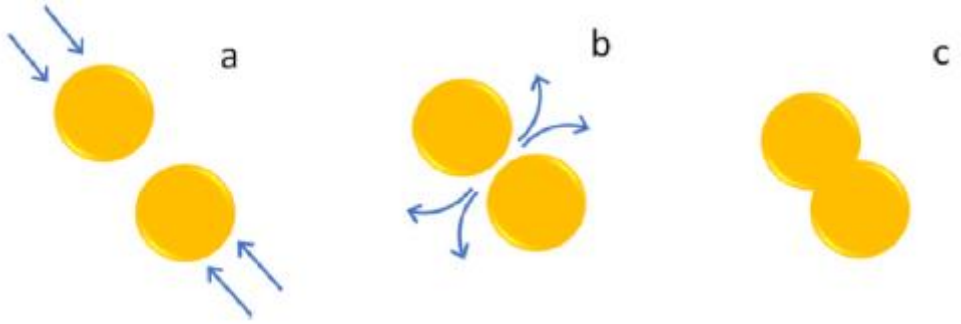

Scheme 3. Schematic droplet coalescence. a) two droplets flow toward each other, b) droplets are approaching and squeeze out the matrix in draining flow, c) the thin film of matrix in draining raptures and droplets coalesce [**26**]

Table 4 The zero uniaxial extensional viscosity η_{e0}, maximum uniaxial extensional viscosity /emax, strain hardening parameter (SH) and Newtonian shear viscosities η_0 of $PMMA/SAN$ blend and composites.

Sample	PMMA/ SAN	GO	GO-PMMA10	GO-PMMA18	GO-PMMA37
η_{e0} (Pa's)	397,500	368,000	278,000	244,000	214,000
η_{emax} (Pa's)	450,100	434,400	382,100	391,600	374,100
SH (—)	1.13	1.18	1.37	1.60	1.75
η_0 (Pa's)	62,700	62,050	62,970	63,580	63,870

The results were correlated with morphology development. Compared to both the neat blend and blend filled with neat GO, the hybrid particles significantly decreased the elongational viscosity at low strains, that facilitated the materials processing. On the other hand, at high strains, the viscosity enhancement was observed. Such material properties are desirable for extrusion and fiber processing, where the melt strength and drawability is required.

6. Conclusion

The effect of molecular parameters of the brushes grafted from GO particles on the rheological properties of $PMMA/SAN$ immiscible blend was investigated. The rheological properties in shear and uniaxial extension were studied. While frequency dependence of complex viscosity analyzed in shear mode did not show significant differences between the samples. TEM analysis revealed the location of GO in SAN phase, while GO-g-PMMA with 10,300 g/mol tended to locate the particles close to the interphase. Increasing M_n of $PMMA$ brushes tended to move the particles in $PMMA$ phase. The compatibilization effect was observed for GO-g-PMMA grafted with 10,300 g/mol brushes. The extensional rheology proved the plasticizing effect of hybrid particles, which was pronounced with increasing length of brushes. The $PMMA/SAN$ blends loaded with GO-g-PMMA, especially with higher molar masses of the $PMMA$ chains, showed improved processability at lower elongation rates ($\sim <$ 0.1 s^{-1}) and improved stability of the melt (melt strength and drawability) at higher elongation rates ($\sim >$ 0.1 s^{-1}).

References

[1] L.A. Utracki, Compatibilization of polymer blends, Can. J. Chem. Eng. 80 (6) (2002) 1008-1016.

[2] J. Stange, C. Uhl, H. Munstedt, Rheological behavior of blends from a linear and a long-chain branched polypropylene, J. Rheol. 49 (5) (2005) 1059-1079.

[3] D.J. Lohse, S.T. Milner, L.J. Fetters, M. Xenidou, N. Hadjichristidis, R. A. Mendelson, C.A. Garcia-Franco, M.K. Lyon, Well-defined, model long chain branched polyethylene. 2. Melt rheological behavior, Macromolecules 35 (8) (2002)3066-3075.

[4] J. Genoyer, J. Soulestin, N.R. Demarquette, Influence of the molar masses on compatibilization mechanism induced by two block copolymers in PMMA/PS blends, J. Rheol. 62 (3) (2018) 681-693.

[5] J. Genoyer, M. Yee, J. Soulestin, N. Demarquette, Compatibilization mechanism induced by organoclay in PMMA/PS blends, J. Rheol. 61 (4) (2017) 613-626.

[6] J.S. Hong, Y.K. Kim, K.H. Ahn, S.J. Lee, C. Kim, Interfacial tension reduction in PBT/PE/clay nanocomposite, Rheol. Acta 46 (4) (2007) 469-478.

[7] F. Ardakani, Y. Jahani, J. Morshedian, Dynamic viscoelastic behavior of polypropylene/polybutene-1 blends and its correlation with morphology, J. Appl. Polym. Sci. 125 (1) (2012) 640-648.

[8] J. Genoyer, N.R. Demarquette, J. Soulestin, Effect of clay particles size and location on coalescence in PMMA/PS blends, J. Rheol. 63 (6) (2019) 883-893.

[9] T. Liu, H.M. Zhang, M. Zuo, W.J. Zhang, W.P. Zhu, Q. Zheng, Selective location and migration of poly(methyl methacrylate)- grafted clay nanosheets with low grafting density in poly(methyl methacrylate)/poly (styrene-co-acrylonitrile) blends, Compos. Sci. Technol. 169 (2019) 110-119.

[10] H.J. Chung, J. Kim, K. Ohno, R.J. Composto, Controlling the location of nanoparticles in polymer blends by tuning the length and end group of polymer brushes, ACS Macro Lett. 1 (1) (2012) 252-256.

[11] H.M. Zhang, M. Zuo, W.P. Zhu, A. Zhao, X.Y. Shi, X.Y. Zhang, Y.H. Song, Q. Zheng, Control of selective location of homopolymer-brush grafted nanoparticles in binary polymer blends, Compos. Sci. Technol. 200 (2020).

[12] C.W. Huang, J.P. Gao, W. Yu, C.X. Zhou, Phase separation of poly(methyl methacrylate)/Poly(styrene-co-acrylonitrile) blends with controlled distribution of silica nanoparticles, Macromolecules 45 (20) (2012) 8420-8429.

[13] L.M. Hu, Y.Y. Han, C.Y. Rong, X.K. Wang, H.T. Wang, Y.J. Li, Interfacial engineering with rigid nanoplatelets in immiscible polymer blends: interface strengthening and interfacial curvature controlling, ACS Appl. Mater. Interfaces 14 (8) (2022) 11016-11027.

[14] J.P. Guan, W.T. Luo, S.F. Lu, Y.R. Yang, X.J. Shen, B.L. Tang, Y.J. Li, Synchronous toughening and strengthening of the immiscible polylactic acid/thermoplastic polyurethane (PLLA/TPU) blends via the interfacial compatibilization with Janus nanosheets, Compos. Sci. Technol. 227 (2022).

[15] H.T. Wang, X. Yang, Z. Fu, X.W. Zhao, Y.J. Li, J.Y. Li, Rheology of nanosilica-compatibilized immiscible polymer blends: formation of a "heterogeneous network" facilitated by interfacially anchored hybrid nanosilica, Macromolecules 50 (23) (2017) 9494-9506.

[16] C.M. Hui, J. Pietrasik, M. Schmitt, C. Mahoney, J. Choi, M.R. Bockstaller, K. Matyjaszewski, Surface-initiated polymerization as an enabling tool for multifunctional (Nano-)Engineered hybrid materials, Chem. Mater. 26 (1) (2014) 745-762.

[17] J.F. Zhang, M. Zuo, X. Lv, H.M. Zhang, Q. Zheng, Effect of grafted graphene nanosheets on morphology evolution and conductive behavior of poly(methyl methacrylate)/poly(styrene-co-acrylonitrile) blends during isothermal annealing, RSC Adv. 8 (26) (2018) 14579-14588.

[18] M. Ilcikova, M. Galeziewska, M. Mrlik, J. Osicka, M. Masar, M. Slouf, M. Maslowski, M. Kracalik, R. Pietrasik, J. Mosnacek, J. Pietrasik, The effect of short polystyrene brushes grafted from graphene oxide on the behavior of miscible PMMA/SAN blends, Polymer 211 (2020).

[19] T.S. Muzata, S. Bose, Polymer tethered graphene oxide influences miscibility and cooperative relaxation in LCST blends, Polymer 188 (2020).

[20] W.B. Huang, T.T. Zhang, J.H. Yang, N. Zhang, T. Huang, Y. Wang, Largely enhanced fracture toughness of an immiscible polyamide 6/acrylonitrile-buta-diene-styrene blend achieved by adding chemically modified graphene oxide, RSC Adv. 5 (123) (2015) 101466-101474.

[21] M. Zygo, M. Lipinska, Z. Lu, M. Ilcikova, M.R. Bockstaller, J. Mosnacek, J. Pietrasik, New type of montmorillonite compatibilizers and their influence on viscoelastic properties of ethylene propylene diene and methyl vinyl silicone rubbers blends, Appl. Clay Sci. 183 (2019).

[22] O. Jankovsky, P. Marvan, M. Novacek, J. Luxa, V. Mazanek, K. Klimova, D. Sedmidubsky, Z. Sofer, Synthesis procedure and type of graphite oxide strongly influence resulting graphene properties, Appl. Mater. Today 4 (2016) 45-53.

[23] M. Galeziewska, A. Holos, M. Ilcikova, M. Mrlik, J. Osicka, P. Srnec, M. Micusík, R. Moucka, M. Cvek, J. Mosnácek, J. Pietrasik, One-pot strategy for the preparation of electrically conductive composites using simultaneous reduction and grafting of graphene oxide via atom transfer radical polymerization, Macromolecules 54 (21) (2021) 10177-10188.

[24] M.H. Wagner, V. Schulze, A. Gottfert, Rheotens-mastercurves and drawability of polymer melts, Polym. Eng. Sci. 36 (7) (1996) 925-935.

[25] M. Khoury, D.K. Ferry, Effect of molecular weight on poly(methyl methacrylate) resolution, J. Vac. Sci. Technol. B 14 (1) (1996) 75-79.

[26] A.T. Hedegaard, L.L. Gu, C.W. Macosko, Effect of extensional viscosity on cocontinuity of immiscible polymer blends, J. Rheol. 59 (6) (2015) 1397-1417.

[27] M. Suess, J. Kressler, H.W. Kammer, The miscibility window of poly(methyl methacrylate) poly(styrene-co-acrylonitrile) blends, Polymer 28 (6) (1987) 957-960.

[28] J.S. Reinaldo, L.M. Pereira, E.D. Silva, M.M. Ueki, E.N. Ito, Effect of the chemical structure on the linear viscoelastic behavior of acrylic and styrenic polymer blends, Polym. Test. 67 (2018) 257-265.

[29] B. Du, U.A. Handge, M. Wambach, C. Abetz, S. Rangou, V. Abetz, Functionalization of MWCNT with P(MMA-co-S) copolymers via ATRP: influence on localization of MWCNT in SAN/PPE 40/60 blends and on rheological and dielectric properties of the composites, Polymer 54 (22) (2013) 6165-6176.

[30] I. Vinckier, H.M. Laun, Manifestation of phase separation processes in oscillatory shear: droplet-matrix systems versus co-continuous morphologies, Rheol. Acta 38 (4) (1999) 274-286.

[31] C. R. Lopez-Barron, C.W. Macosko, Rheology of compatibilized immiscible blends with droplet-matrix and cocontinuous morphologies during coarsening, J. Rheol. 58 (6) (2014) 1935-1953.

[32] R.M. Li, W. Yu, C.X. Zhou, Rheological characterization of droplet-matrix versus co-continuous morphology, J. Macromol. Sci., Part B: Phys. 45 (5) (2006) 889-898.

[33] H. Gramespacher, J. Meissner, Interfacial tension between polymer melts measured by shear oscillations of their blends, J. Rheol. 36 (6) (1992) 1127-1141.

[34] C.R. Lopez-Barron, C.W. Macosko, Rheological and morphological study of cocontinuous polymer blends during coarsening, J. Rheol. 56 (6) (2012) 1315-1334.

[35] C.R. Lopez-Barron, C.W. Macosko, Characterizing interface shape evolution in immiscible polymer blends via 3D image analysis, Langmuir 25 (16) (2009) 9392-9404.

[36] W. T.N, The Phenomenological Theory of Linear Viscoelastic Behavior an Introduction, Springer, Berlin, 1989.

[37] M.H. Wagner, A. Bernnat, V. Schulze, The rheology of the rheotens test, J. Rheol. 42 (4) (1998) 917-928.

[38] G.X. Liu, H. Sun, S. Rangou, K. Ntetsikas, A. Avgeropoulos, S.Q. Wang, Studying the origin of "strain hardening": basic difference between extension and shear, J. Rheol. 57 (1) (2013) 89-104.

[39] M. Galeziewska, M. Lipinska, M. Mrlik, M. Ilcikova, V. Gajdosova, M. Slouf, E. Achbergerova, L. Musilova, J. Mosnacek, J. Pietrasik, Polyacrylamide brushes with varied morphologies as a tool for control of the intermolecular interactions within EPDM/MVQ blends, Polymer 215 (2021).

[40] K. Yasuda, R.C. Armstrong, R.E. Cohen, Shear flow properties of concentrated solutions of linear and star branched polystyrenes, Rheol. Acta 20 (2) (1981) 163-178.